JOURNAL OF GEOPHYSICAL RESEARCH, VOL. 106, NO. A6, PAGES 10,493–10,508, JUNE 1, 2001

Assimilated observations of thermospheric winds, the aurora, and ionospheric currents over Alaska

M. Conde, J. D. Craven, T. Immel[1], E. Hoch, H. Stenbaek-Nielsen, T. Hallinan, R. W. Smith, J. Olson, and Wei Sun

Geophysical Institute, University of Alaska Fairbanks

L. A. Frank, and J. Sigwarth

Department of Physics and Astronomy, University of Iowa, Iowa City

Abstract. We present simultaneous measurements of thermospheric winds, auroral emissions, and ionospheric currents over Alaska, obtained from four separate instruments. Thermospheric (F region) wind maps were recorded by an all-sky imaging Fabry-Perot spectrometer located at Poker Flat and observing at λ630.0 nm. Auroral images at λ557.7 nm were obtained from the low-resolution visible imager on board the Polar satellite. White-light all-sky auroral images were recorded by ground-based all-sky cameras located in Alaska at Poker Flat (65° 07′N, 212° 34′E) and at Kaktovik (70° 06′N, 217° 24′E). Finally, the east-west component of the ionospheric F region plasma convection was inferred using the Alaskan meridian chain of magnetometers. Montage images of these four data sets are presented, projected onto a geographic map of the Alaskan region. We examine a 10-hour period during the Alaskan local nighttime of February 10, 1997. These montages illustrate a close relationship between spatial structures occurring in the aurora, in the ionospheric plasma convection, and in the F region wind field. Latitudinal shear of the geomagnetic zonal wind, often observed in the premidnight time sector, was seen to be associated with both the equatorward and poleward boundaries of the discrete aurora. We focus particularly on a period commencing just after 0900 UT, when a strong shear in the zonal wind was observed to sweep southward across Alaska. After magnetic midnight the wind field was dominated by the emergence of the "cross-polar jet" from the polar cap. This overwhelmed any wind features associated with local auroral processes.

1. Introduction

Winds in the Earth's thermosphere above ~100-km altitude have been measured by various methods since the 1960s. Over Alaska, for example, thermospheric winds have been measured using ground-based Fabry-Perot spectrometers [*Nagy et al.*, 1974; *Hays et al.*, 1979; *Sica et al.*, 1986a, 1989, 1993; *Smith et al.*, 1989], rocket-borne chemical releases [*Meriwether et al.*, 1973; *Mikkelsen et al.*, 1981; *Heppner and Miller*, 1982; *Larsen et al.*, 1995, 1997], incoherent scatter radar [*Bates and Roberts*, 1977; *Wickwar et al.*, 1984], and the Dynamics Explorer 2 satellite [e.g., *Killeen and Roble*, 1988]. Many of these measurements have focused on the upper thermosphere, in the height range ~200-600 km, mostly because the simplest experimental techniques work best at these altitudes.

Paralleling these observational campaigns has been the development of sophisticated first-principles three-dimensional, time-dependent thermospheric computer models [*Fuller-Rowell and Rees*, 1980; *Dickinson et al.*, 1981; *Fuller-Rowell et al.*, 1987; *Roble and Ridley*, 1987; *Roble et al.*, 1988; *Richmond et al.*, 1992; *Idenden et al.*, 1996]. Taken together, the observational and modeling developments have yielded a widely accepted picture of the "large-scale" behavior of winds in the upper thermosphere. However, the horizontal resolution achieved by most studies, both observational and modeling, has been limited by available instrumental and computer resources to spatial scales of typically ~500 km or larger.

The Dynamics Explorer 2 satellite was able to measure all three components of the wind vector as functions of distance along the satellite track. These measurements showed that there is a close association between reversals and boundaries in the neutral wind and the location of the aurora [e.g., *Spencer et al.*, 1982; *Hays et al.*, 1984; *Killeen et al.*, 1988]. This result

[1]Now at Space Sciences Laboratory, University of California Berkely, CA 94720-7450

Paper number 2000JA000135.
0148-0227/01/2000JA000135$09.00

is consistent with the predictions of simplified two-dimensional atmospheric models running at high spatial resolution, which suggest that strong shears may develop in the thermospheric wind field within several hundred kilometers of an auroral arc [*St.-Maurice and Schunk*, 1981; *Fuller-Rowell*, 1985; *Lyons and Walterscheid*, 1985; *Walterscheid et al.*, 1985; *Chang and St.-Maurice*, 1991; *Walterscheid and Lyons*, 1992; *Keskinen and Satyanarayana*, 1993].

Although DE 2 did measure all three components of the thermospheric wind, it only resolved the spatial variation of the vector wind field with respect to one spatial dimension (i.e., along the satellite track). Further, the spatial resolution of the DE 2 meridional wind data was limited to typically ~500 km by the satellite's limb-viewing geometry [*Killeen and Roble*, 1988]. Also, for a given location the DE 2 measurements only provided isolated instantaneous measurements, occurring during individual satellite overpasses.

The Poker Flat thermospheric wind imaging project was initiated in 1995, with the objective of obtaining upper thermospheric wind observations down to scale lengths significantly shorter than 500 km. A novel wavelength scanning, all-sky imaging Fabry-Perot spectrometer (ASI-FPS) was developed to facilitate these measurements [*Conde and Smith*, 1997]. Earlier all-sky Fabry-Perot instruments [*Rees and Greenaway*, 1983; *Biondi et al.*, 1995; *Nakajima et al.*, 1995] have used fixed-gap etalons to derive wavelength spectra from the shapes of the Fabry-Perot fringes. Unfortunately, such spectra are susceptible to distortions in the presence of aurora, owing to intensity gradients across the sky. The Poker Flat ASI-FPS uses a separation-scanned etalon to recover spectra as a function of etalon gap (rather than fringe shape) and is insensitive to spatial intensity gradients in the aurora. We had postulated that small-scale processes, particularly those associated with the aurora, would establish wind structures that varied over length scales as short as 100 km. Early observational results from the ASI-FPS instrument rapidly confirmed the existence of these small-scale wind structures [*Conde and Smith*, 1995, 1998a, 1998b].

Recent work on this project is now focused on presenting an assimilated description of the Alaskan ionosphere and thermosphere, by combining ASI-FPS wind measurements with data from several other preexisting ground- and space-based instruments. An example of this assimilation work is presented here. Our immediate goal is to understand what processes establish the observed small-scale wind features. In the longer term we hope to examine the significance of small-scale flow structures in dissipating the energy and momentum supplied to the thermosphere by the solar wind, via the magnetosphere and ionosphere.

2. Instrumentation

2.1. All-Sky Imaging Fabry-Perot Spectrometer

The Poker Flat wind mapper is an all-sky imaging Fabry-Perot spectrometer (ASI-FPS) with separation-scanned etalon plates. It views the sky down to 65° zenith angle and divides this field of view into a contiguous set of "zones," typically 25 or 31 in number. An independent spectrum is acquired from each zone and analyzed for Doppler shifts and Doppler widths. Doppler shifts yield estimates of the line-of-sight wind component prevailing in each viewing zone. Here we have recorded and analyzed spectra of the thermospheric λ630 nm atomic oxygen emission. Thus the inferred winds are representative of conditions at 240-km altitude [e.g., *Sica et al.*, 1986b]. For the instrument configuration used during the February 1997 period presented here, wind estimates were obtained in each of the 25 zones with a typical uncertainty of ~20 $\mathrm{m\,s^{-1}}$ using exposure times of 15 min. (The imaging detector was upgraded in 1998 to an intensified CCD, yielding typical performance of 10 $\mathrm{m\,s^{-1}}$ wind uncertainty over 31 zones, from exposure times of only 6 min.) The instrument and observing techniques are described fully by *Conde and Smith* [1995, 1997, 1998b].

Doppler shifts of the emission spectra only yield estimates of the line-of-sight component of the wind. To infer a unique two-dimensional vector horizontal wind field from a single observing site requires additional assumptions, as described by *Conde and Smith* [1998b]. Briefly, we calculate a simple model (H_x, H_y) of the horizontal vector wind field using first-order Taylor series expansions of the zonal (u) and meridional (v) components about the zenith point above an observatory,

$$H_x = u_0 + \frac{\partial u}{\partial x}x + \frac{\partial u}{\partial y}y, \tag{1}$$

$$H_y = v_0 + \frac{\partial v}{\partial x}x + \frac{\partial v}{\partial y}y, \tag{2}$$

where x and y are the zonal and meridional distances from the zenith to an observation point viewed at zenith angle ϕ and azimuth angle θ, i.e.,

$$x = R\sin\theta, \tag{3}$$

$$y = R\cos\theta, \tag{4}$$

$$R = h\tan\phi, \tag{5}$$

with h being the height of the emission layer. The model wind field is described by six coefficients, u_0, $\partial u/\partial x$, $\partial u/\partial y$, v_0, $\partial v/\partial x$, and $\partial v/\partial y$. These coefficients are

chosen to give the best fit between the line-of-sight components observed in the real wind field and the corresponding line-of-sight components calculated from the model. Unfortunately, observations from a single site do not yield a unique solution for all six coefficients, no matter how many viewing directions are used. Thus an additional constraint is obtained by assuming that, at least over short time intervals,

$$\frac{\partial v}{\partial x} \simeq \frac{1}{\epsilon}\frac{\partial v}{\partial t}, \tag{6}$$

where ϵ is the tangential velocity of the observatory due to the rotation of the Earth [*Burnside et al.*, 1981]. The assumption is that for sufficiently short time intervals the rotation of the Earth can be regarded as moving the station through a meridional wind field that is stationary in local time. This allows the meridional wind to be sampled at various locations along the zonal direction, which is not possible using line-of-sight data from a single observation. Although this assumption may be violated when the wind field is changing rapidly with time, *Conde and Smith* [1998b] argue that, in practice, instances of significant distortions due to this effect are rare.

2.2. Polar Visible Imaging System

The Visible Imaging System (VIS) aboard the Polar spacecraft has been described by *Frank et al.* [1995]. It comprises a set of three low-light-level cameras, two of which provide images of the nighttime auroral oval at visible wavelengths, while the third is used to monitor the directions of viewing with respect to the sunlit Earth and coincidentally provides global-scale images of the aurora at FUV wavelengths. The two auroral cameras have single-pixel dimensions of ~10 and 20 km from a spacecraft altitude of 8 R_E. A number of different auroral emissions can be observed using narrowband filters. Here we present λ557.7 nm images. The time assigned to each 256×256 pixel image acquired with the low-resolution auroral camera corresponded to the time at the end of the image readout from the CCD. The exposure of these images began 28 s earlier and lasted for 24 s. The images that we used here had already been mapped onto a uniform longitude-latitude grid. Not all of the original images had been processed this way; however, mapped images were readily available at 6-7 min intervals, which is about twice the measurement frequency of the ASI-FPS data.

2.3. Poker Flat All-Sky Camera

The ground-based all-sky cameras (ASC) at Poker Flat and Kaktovik (described by *Kimball and Hallinan* [1998a, 1998b]) are lens-coupled, intensified CCD systems. The Poker Flat camera operates automatically whenever the moon is set and the Sun is at least 13° below the horizon, whereas the Kaktovik camera is operated solely on a campaign basis. The cameras normally operate unfiltered and are sensitive throughout the visible spectrum. Images are recorded on VHS videotape at 30 Hz and are also digitized by computer once per minute. Here we obtained our all-sky camera images from the 1-min time resolution digital archive. The digitized images (and time-lapse movies compiled from them) are freely available via the internet at http://gedds.pfrr.alaska.edu/allsky/.

A ground-based camera can only observe a restricted portion of the auroral oval, whereas spacecraft like Polar can image the aurora over an entire hemisphere. However, the ground-based perspective is much better for observing the auroral fine structure that is associated with local coupling phenomena.

2.4. Magnetometer-Derived Electrojet Current

Magnetic H component values recorded along a meridional chain of sites can be inverted to estimate the one-dimensional east-west component of the auroral electrojet current density (EJT) along the meridian [*Sun et al.*, 1993]. We have applied this technique to an Alaskan meridian chain of magnetometers, which comprised stations at Kaktovik, Fort Yukon, College, Talkeetna, and Anchorage. The geographic locations of these sites are printed in Table 1 and plotted in Figure 1. More information on the stations is available over the World Wide Web at http://magnet.gi.alaska.edu/. The electrojet calculation was run using the highest time resolution magnetometer data available, i.e., at 1-min intervals.

The auroral electrojets arise in the E region, where ion motion is retarded by collisions but electrons continue to move freely in the $\mathbf{E} \times \mathbf{B}$ direction. The differential motion of ions and electrons results in a current. At the height of maximum current density the electron velocity significantly exceeds that of the ions. Thus the electrojet current is carried mostly by the E region horizontal electron flux, and it is directed approximately opposite to the electron velocity. In the F region, however, ions and electrons move together. Thus we have assumed that by simply reversing the sign of the E region electrojet current density, we can obtain a crude and qualitative proxy for the (horizontal) F region ion convection.

3. Data Assimilation

We have only attempted to assimilate the data graphically. All of the contributing instruments returned data that were resolved spatially over at least one dimen-

Table 1. Locations of Magnetometer Stations

Station	Geographic Latitude, deg	Geographic Longitude, deg	Magnetic Latitude	Magnetic Longitude
Kaktovik	70.1	217.4	71.0	260.3
Fort Yukon	66.6	214.8	66.7	262.2
College	64.9	212.2	64.9	261.6
Talkeetna	62.3	209.9	62.0	261.6
Anchorage	61.2	210.1	60.9	259.1

sion, i.e., latitude. Three of the four (ASI-FPS, VIS, and ASC) also resolved their measurements in longitude. Thus a convenient way to overlay all of the data sets was to superimpose them onto a geographic map of the Alaskan region.

The four data sets were computer rendered as bit map images, using a simple projection in which distances east and north from Poker Flat mapped linearly to x and y distances from the center of the bit map. The geographic maps presented here were also generated as bit map images, but in this case using an azimuthal equidistant projection covering the Alaskan region (the projection origin was chosen to lie at the intersection of the equator and the meridian of Poker Flat). Then, for each pixel in the geographic map, the azimuthal equidistant projection was inverted to calculate the longitude and latitude of that pixel. These (longitude, latitude) coordinates were used to "look-up" the corresponding pixel in the each of the linearly projected data bit maps. Provided that the chosen pixel of a data bit map did not contain a "no observation" value, that data value was then overlaid onto the current pixel location of the geographic map. The observational data were overlaid in the following sequence: VIS, ASC, EJT, and ASI-FPS. Thus ASC data appear on top of VIS data, etc. Finally, the coastlines were redrawn over the composite image, to repair gaps made by the overlaid data.

The transformation to an azimuthal projection yielded a visually pleasing map format, albeit at the expense of making the ASI-FPS and ASC field of view circles appear slightly "egg" shaped, and of slightly curving the zero-deflection axis of the EJT plots. Positional uncertainties are inevitably introduced when projecting the various data sets onto a geographic map. These uncertainties are different for each experiment and in most cases vary across the field of view of even a single instrument. We have not attempted to quantify these variations; rather, we merely note that the positional uncertainties are small compared to the length scale of the smallest spatial structures that we observe in the F

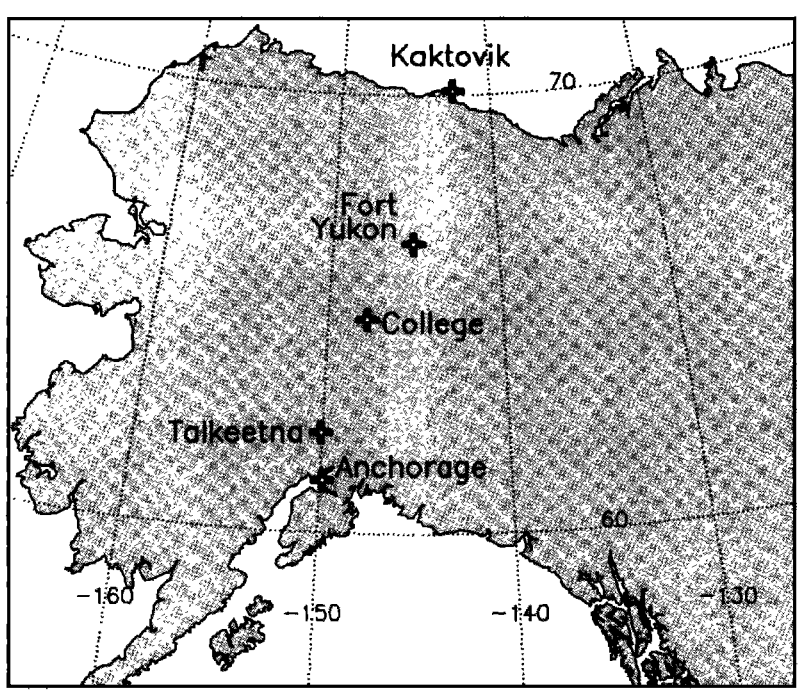

Figure 1. A map of Alaska showing the locations of ground-based magnetometer stations contributing data to the electrojet calculations.

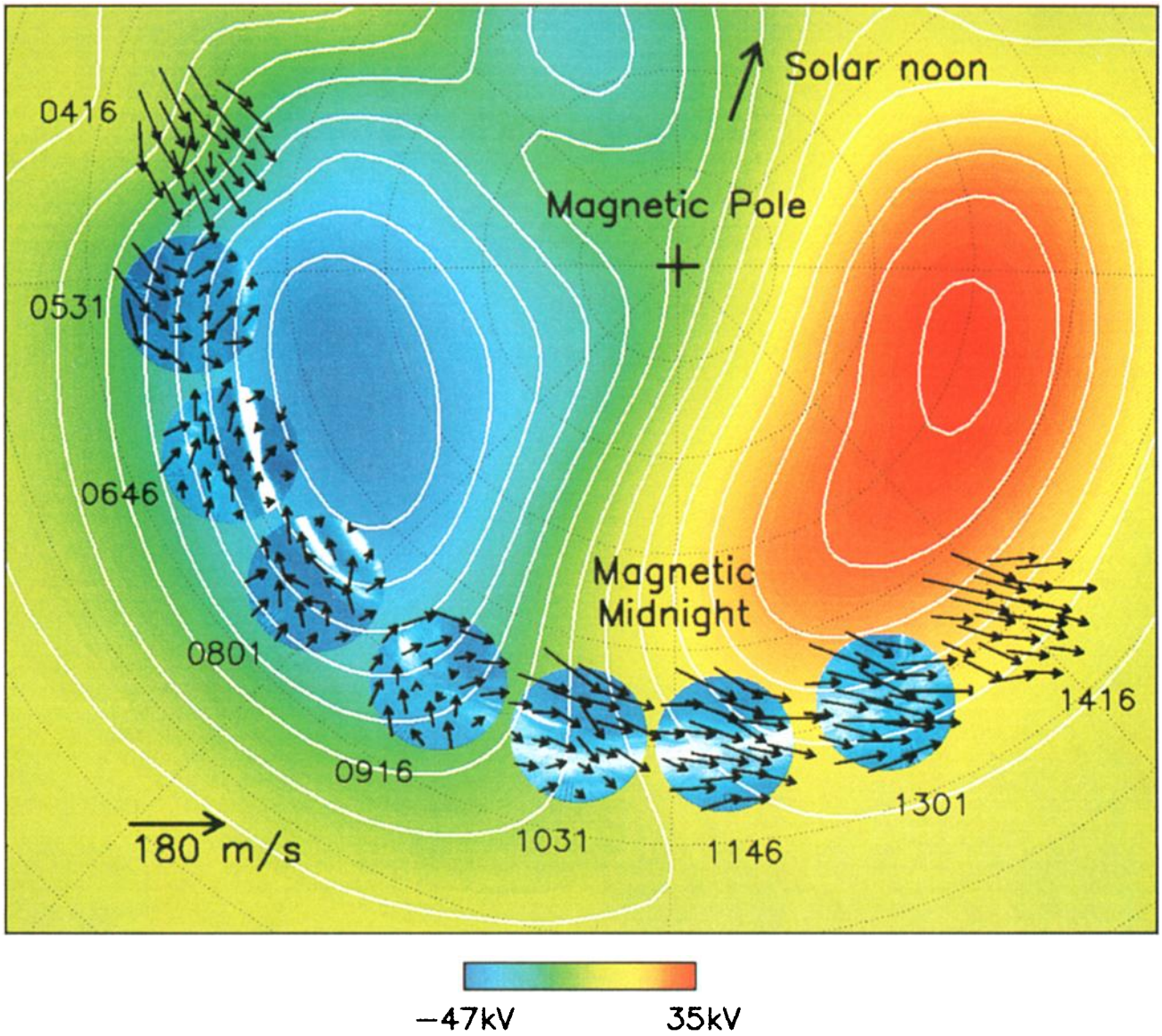

Plate 1. A polar view of the local-time evolution of the thermospheric wind field above Poker Flat on February 10, 1997, superimposed on Poker Flat all-camera images and on a representation of the local-time evolution of the *Weimer* [1995] convection model. This presentation is explained in more detail in the text.

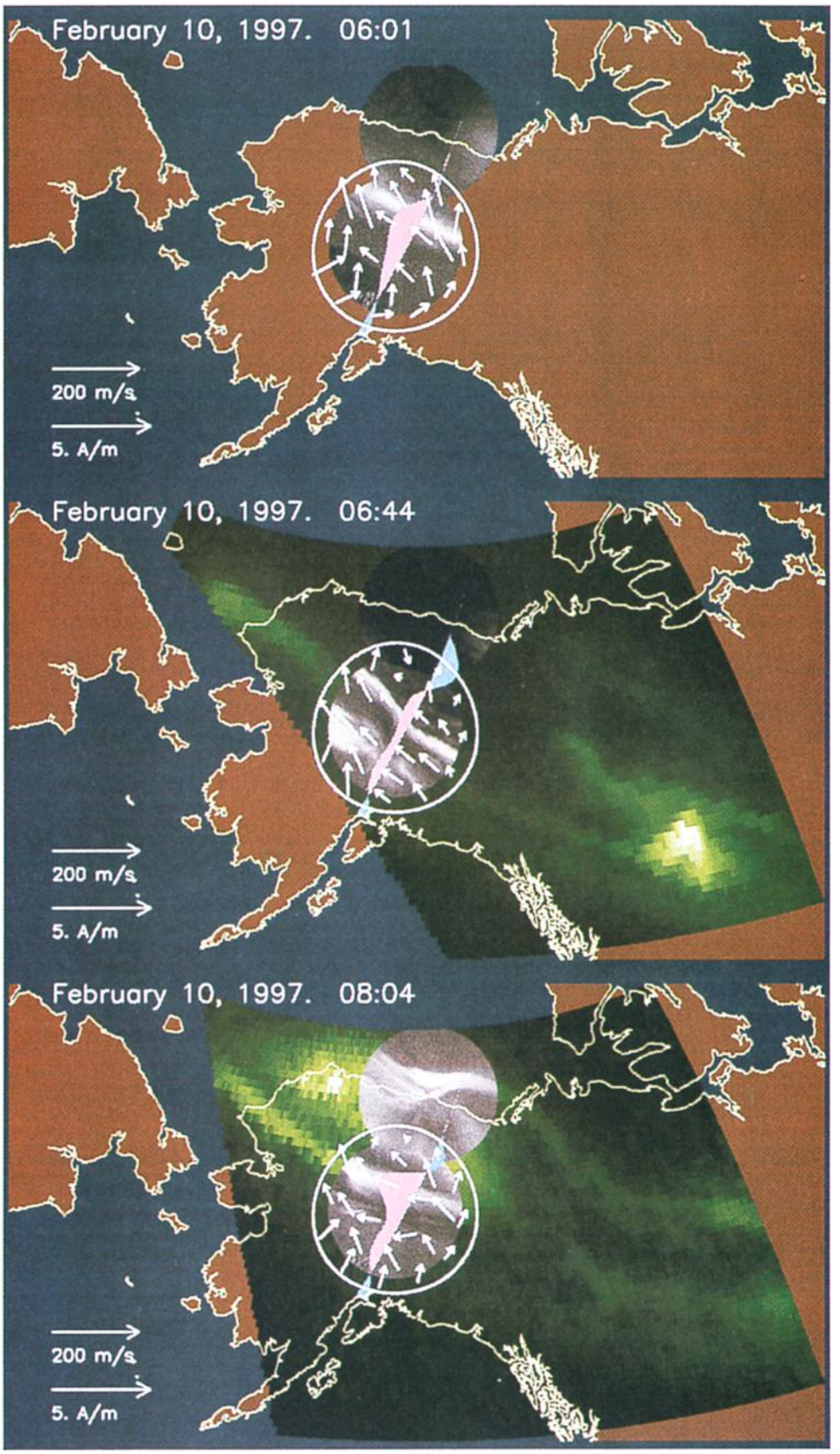

Plate 2. Data from the Fabry-Perot spectrometer, ground-based all-sky cameras, Polar Visible Imaging System (VIS) camera, and the electrojet calculation, overlaid as described in the text. The three panels correspond to three times during the early evening of February 10, 1997.

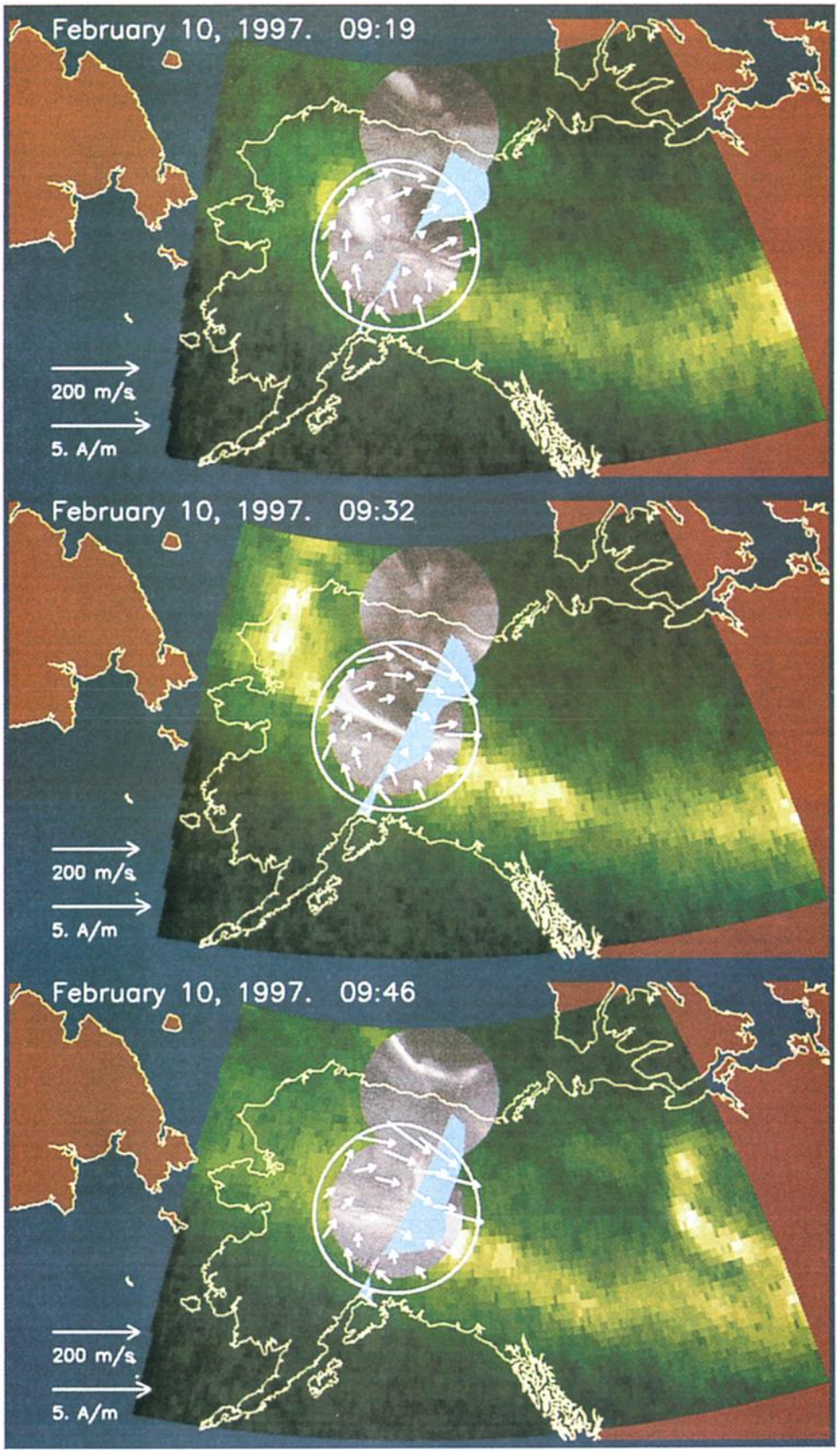

Plate 3. Data overlaid as described in the text, for the period 0919-0946 UT.

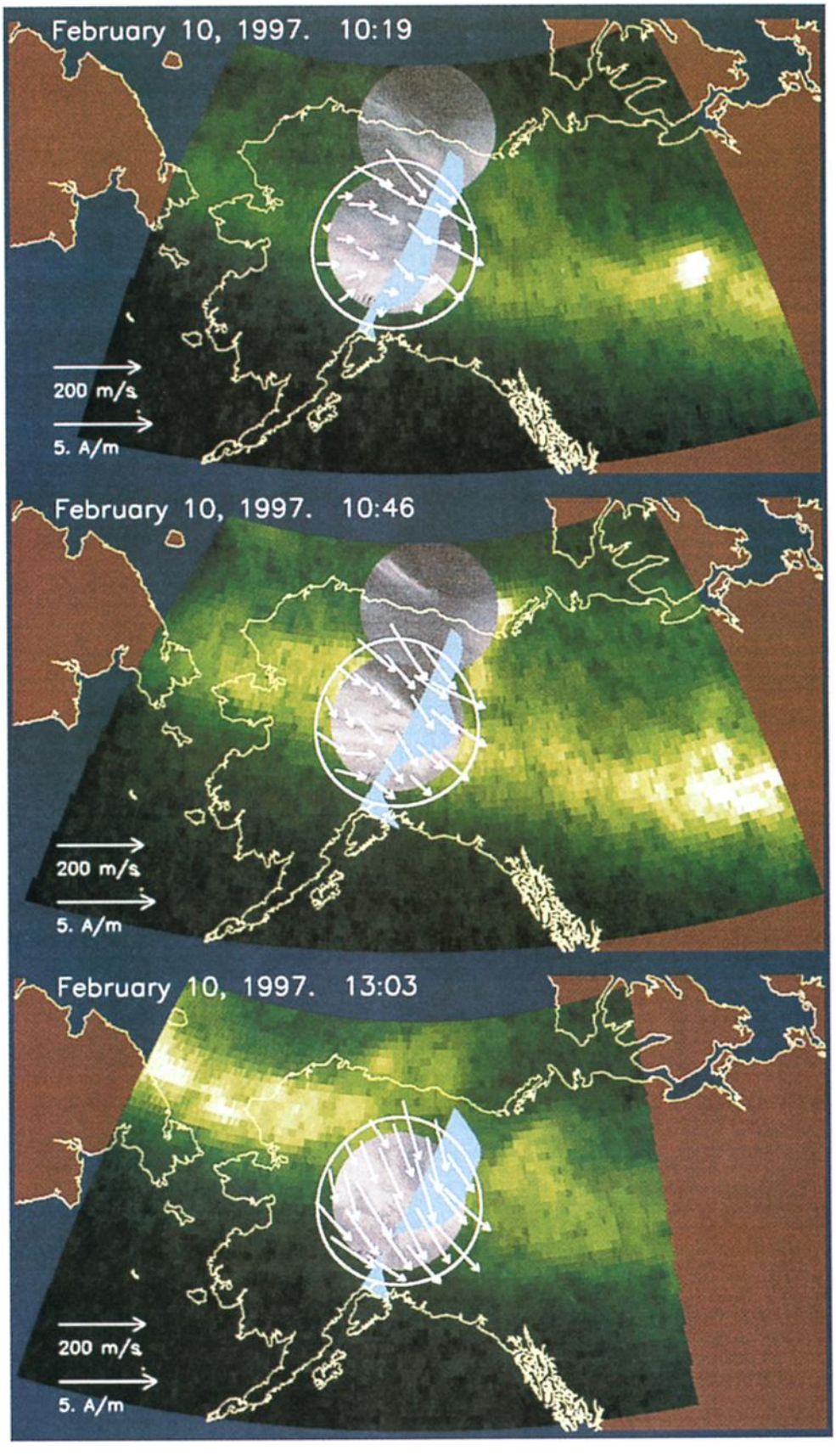

Plate 4. Overlaid data for the period 1019-1303 UT.

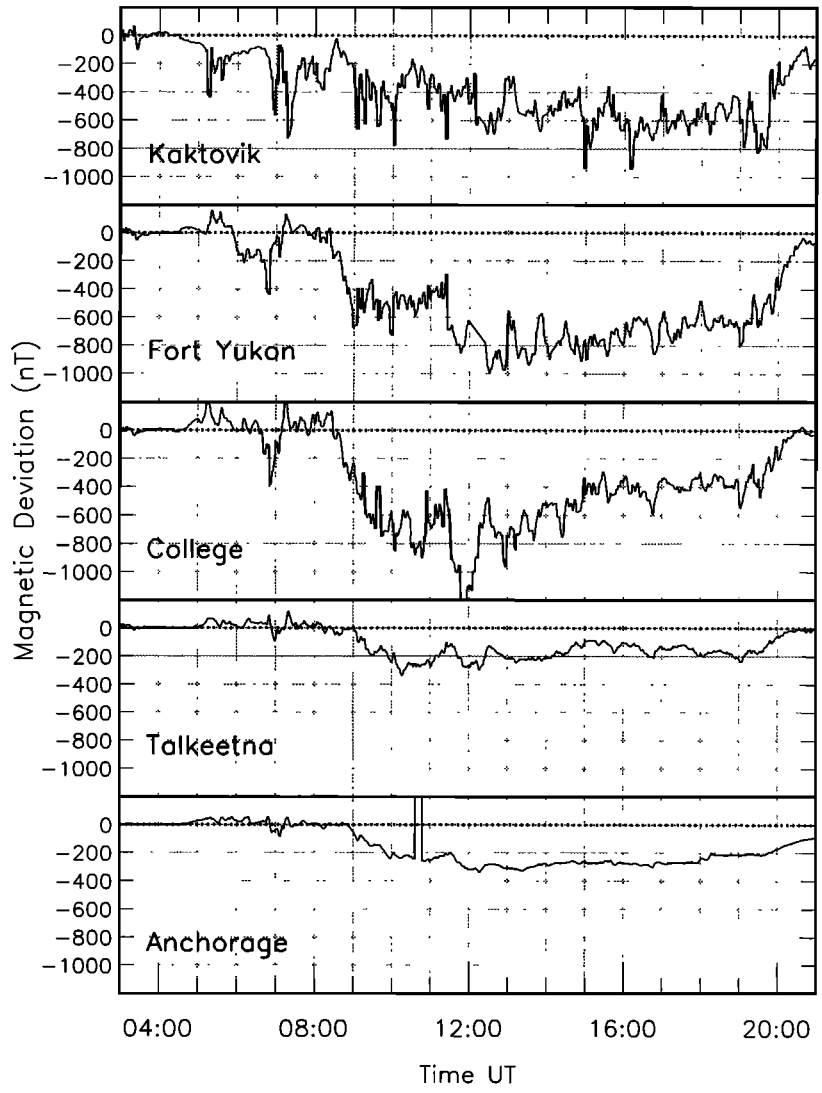

Figure 2. Magnetometer H component traces for February 10, 1997, from the meridian chain of stations described in the text.

region wind field.

The ASI-FPS exposure time of 15 min yielded the slowest data update rate of the four instruments. Thus we could only make the assimilation maps at ~15-min intervals. Even so, the 8-hour time period that we examined yielded 33 maps, far too many for all to be included here. Thus we have only presented here a few selected examples to illustrate the important coupling phenomena evident in these data. We focus particularly on a period commencing just after 0900 UT, when a strong shear in the zonal wind was observed to sweep southward across Alaska.

The time assigned to each of the maps was based initially on the central time of the ASI-FPS exposure. Since the set of geographically mapped VIS images that we used here were sampled every 6 to 7 min, these data had the second lowest time resolution of the four instruments. Thus we next found the VIS image closest in time to each ASI-FPS exposure's central time. The exposure time of the selected VIS image was then used as the time stamp for the whole assimilation. The ASC and EJT data were available to us every minute; the closest ASC and EJT data to the selected VIS time were then chosen to be added to the assimilation. The consequence of this procedure was that the VIS, ASC, and EJT data always match in time to within ~1 min; however, this time may be displaced up to 3-4 min from the central time of the associated ASI-FPS exposure.

The time constant for the thermospheric wind to respond to a change in ion-drag forcing is usually assumed to be 1 hour or more [e.g., *Killeen et al.*, 1984; *Meriwether et al.*, 1988], except in regions of enhanced electron density such as the cusp and the evening auroral zone [*Smith et al.*, 1988]. Our own ASI-FPS observations span hundreds of nights, with time resolution in some cases down to 4 min. These observations often contain examples of changes on timescales as short as 30 min, or less. However, we have never observed the F region wind field change so rapidly that the 3-4 min "time jitter" in matching the ASI-FPS wind data to

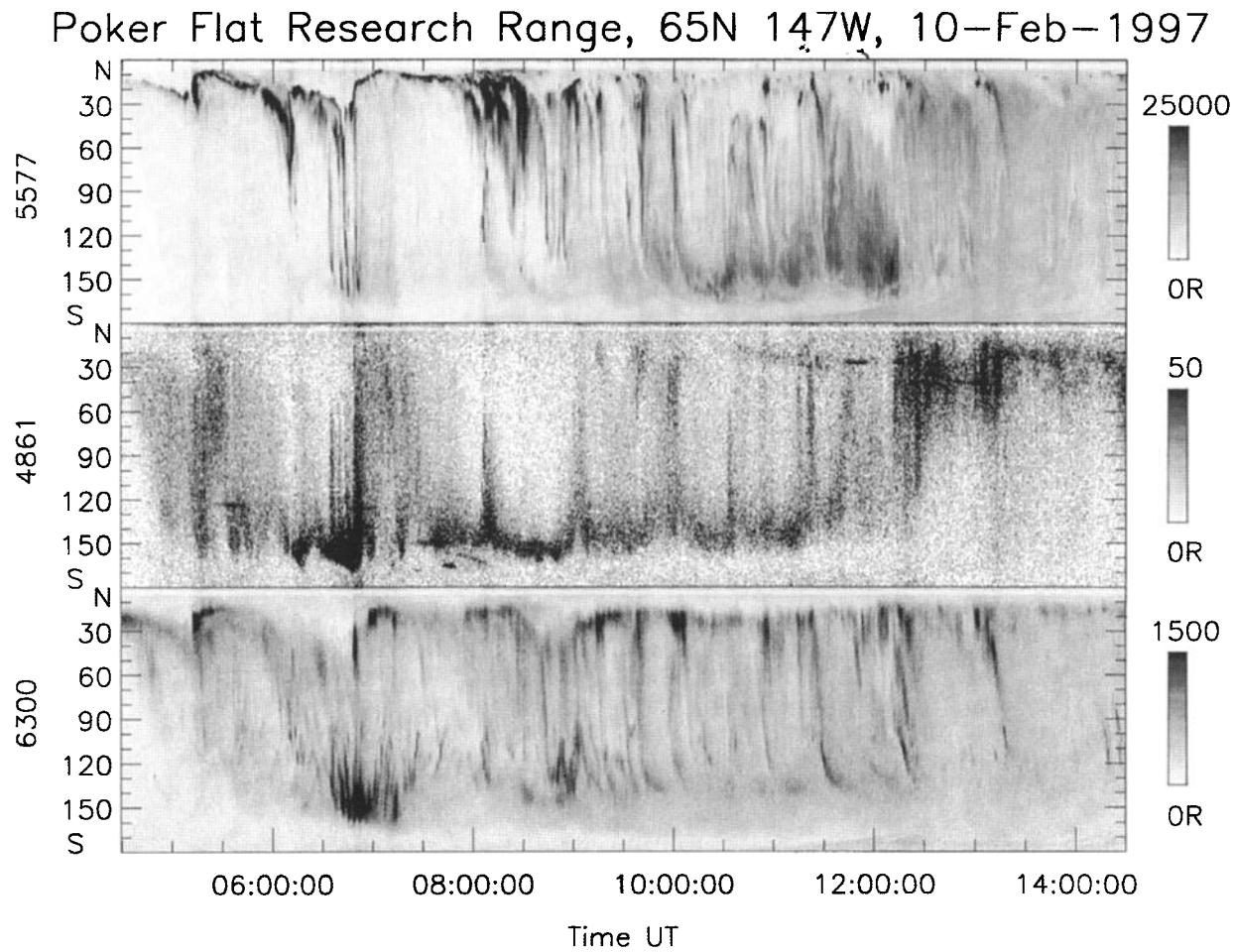

Figure 3. Poker Flat meridian-scanning photometer data for the night of Februrary 10,1997. A rotating mirror in this instrument sweeps the fields of view of four photometers along the local magnetic meridian from the north to the south horizon. The photometers measure the auroral brightness at four wavelengths (of which only three are shown here.) The horizontal axis is universal time, whereas the vertical axes indicate the viewing angle in the sky, measured from 0 at the north horizon. Gray scale bars indicate the intensity scale at each wavelength.

VIS, ASC, and EJT observations would introduce significant discrepancies.

In all cases we will refer to observation times using the universal time system. Similarly, unless otherwise stated, all directions will be quoted relative to geomagnetic north, which is ~25° east of geographic north at Poker Flat. (Geomagnetic north is easily visualized on auroral images, as it lies perpendicular to the general geomagnetic east-west alignment of the large-scale auroral forms.)

4. Observations

4.1. Geophysical Conditions on February 10, 1997

We present data from the 10-hour period from 0416 to 1416 UT on February 10, 1997. Globally, this was a moderately disturbed day, with the 3-hour Kp indices being 4_-, 4_-, 4_0, 3_+, 3_+, 3_+, 4_0, and 4_-. Locally, however, auroral and magnetic conditions reached storm levels for many hours, as is apparent from the meridian chain magnetometer data shown in Figure 2 and the four-channel meridian-scanning photometer (MSP) data shown in Figure 3.

The solar wind speed of 400-500 $\mathrm{km\,s^{-1}}$ was ~150 $\mathrm{km\,s^{-1}}$ above its quiescent value throughout the period studied here. Figure 4 shows the x, y, and z components of the interplanetary magnetic field, in GSM coordinates, for February 10, 1997. These data were recorded by the Wind spacecraft, from a location ~200 R_E (or ~45 min) "upstream" of the Earth with respect to the solar wind. The interplanetary magnetic field (IMF) B_z component was persistently negative, varying between 4 and 8 nT southward.

The daily $F_{10.7}$ solar radio flux index was 70.4, and the 30-day average $F_{10.7}$ solar radio flux index was 72.5, indicating that this should definitely be regarded as a solar minimum period. Apart from a cloud band ap-

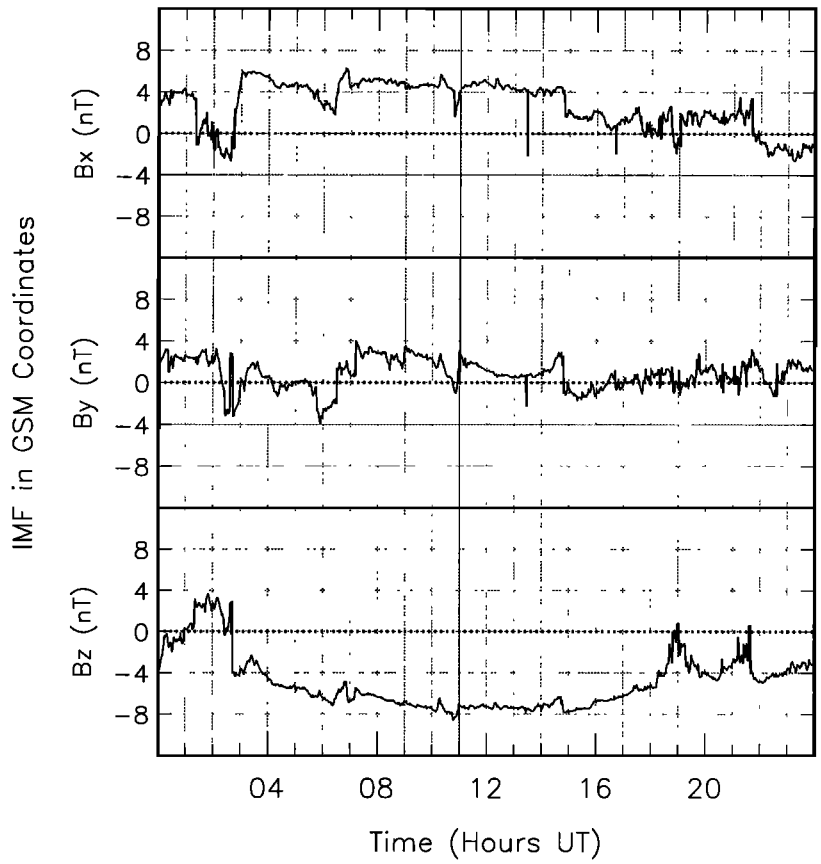

Figure 4. Interplanetary magnetic field (IMF) measurements from the Wind spacecraft for February 10, 1997. The horizontal axis indicates the time of spacecraft measurement, which is ~45 min prior to the corresponding solar wind arrival time at Earth.

pearing low in the south late in the night, the skies were clear above interior Alaska, offering ground-based optical instruments a good view of the thermosphere.

4.2. Overview of Neutral Winds on February 10, 1997

In order to provide an overview and context for the discussion that follows, Plate 1 is a summary plot of the neutral wind variation during the Alaskan night of February 10, 1997. The "clock dial" layout of this plot is similar to that often used to display thermospheric winds recorded at high-latitude sites, except that in this case the black arrows show complete sky maps of the wind field as a function of time, rather than the traditional one or two vectors for each time. Plate 1 is intended to show the evolution of the wind field above Poker Flat as seen by an observer located in space, some distance above the north geomagnetic pole. The direction to the Sun is at the top of Plate 1 so as time advances, the spaced-based observer would see the observatory move anticlockwise in a circular arc centered on the magnetic pole. Each successive set of vectors in a circle maps the wind field measurable from Poker Flat, at ~75 min intervals, and is labeled with the corresponding universal time. (Although we observed winds using 15-min exposures, Plate 1 can only show every fifth exposure without overlap, because the field of view has been depicted at the correct scale relative to the distance to the magnetic pole.)

The blue-white background images in Plate 1 are Poker Flat all-sky camera images mapped onto Plate 1's coordinate system. The rainbow image and associated white contours were derived by evaluating the ionospheric electric field model of *Weimer* [1995]. It must be emphasized that Plate 1 does not depict an instantaneous map of the ionospheric electric potential. Rather, each "meridian" in Plate 1 maps to a different magnetic local time at Poker Flat. Thus universal time increases anticlockwise around Plate 1, as is apparent from the time stamps drawn next to each wind map. Plate 1 was generated by determining the universal time corresponding to each pixel and then calculating the *Weimer* [1995] electric potential at that pixel, based on the IMF and the solar wind speed corresponding to that time. The IMF and solar wind data were obtained from Wind spacecraft measurements, suitably lagged to allow for the solar wind's transit time from the spacecraft to the Earth. The electric potential discontinuity at ~15 hours magnetic local time in Plate 1 arises because regions either side of this were calculated

using IMF and solar wind data separated by 24 hours of universal time.

Plate 1 is only based on a statistical electric field model and cannot be expected to reproduce small-scale features occurring on a particular day. Nevertheless, the general effects of ion convection on the neutral wind are very apparent. The transition from antisunward to sunward neutral flow is seen between 0531 and 0801 UT. This is the signature of ion drag transferring westward momentum to the neutral wind from the duskside ion convection. From 0916 UT onward the influence of the cross-polar convection is also obvious, shearing the neutral flow back toward the eastward direction.

4.3. 0601 UT

In the early evening (before ~0500 UT) the dusk auroral oval usually lies well north of Poker Flat. At solar minimum, and unless geomagnetic storm conditions have prevailed for several hours, F region winds are driven mainly by solar-UV-induced global pressure gradients. As the winter Sun sets in the (geographic) west-southwest, the antisolar pressure gradient drives uniform winds that blow toward the (geographic) east or northeast [*Conde and Smith*, 1998b]. This was the flow configuration that prevailed on February 10 at 0416 UT, at the start of this night's observations, as can be seen in the wind field labeled 0416 in Plate 1.

The MSP data shown in Figure 3 indicate that the diffuse aurora gradually expanded equatorward throughout the hour or so before 0500 UT. Between 0500 and 0600 UT, diffuse aurora covered the whole sky, with the λ486.1-nm emissions from precipitating protons reaching a maximum well south of Poker Flat. By 0601 UT a bright discrete auroral arc had become prominent to the north of Poker Flat, as can been seen in the ASC data mapped as two adjacent gray scale images in the top panel of Plate 2. (Poker Flat lies at center of the lower of the two mapped ASC images.)

Fabry-Perot wind measurements are depicted by white arrows in Plate 2. A strong geomagnetically westward shear with increasing geomagnetic latitude is apparent in the F region wind measurements at 0601 UT. Presumably, this shear was established by westward directed ion drag, which is expected to be associated with the dusk auroral oval [*St.-Maurice and Schunk*, 1981; *Fuller-Rowell*, 1985; *Lyons and Walterscheid*, 1985; *Walterscheid et al.*, 1985; *Chang and St.-Maurice*, 1991; *Walterscheid and Lyons*, 1992].

Note that the westward wind was spatially coincident with the discrete aurora. However, the latitude of strongest westward shear coincided with that of the diffuse aurora, which lay equatorward of the discrete aurora. The region of strongest shear presumably corresponds to the region of greatest ion-neutral momentum transfer. This is consistent with the ion convection profile, inferred from the electrojet, and shown as the curve filled with blue (westward) or pink (eastward) shading in Plate 2. Although the inferred westward convection maximized near the equatorward boundary of the discrete aurora, its latitudinal profile was significantly asymmetric, with the profile's centroid lying well within the region of diffuse aurora. Poker Flat was not yet visible to the POLAR satellite at this time (owing to its orbital position), so the only auroral images included in the upper panel of Plate 2 were from the Poker Flat and Kaktovik ASC instruments.

4.4. 0644 UT

The MSP data in Figure 3 show that an equatorward expansion of the aurora began at around 0630 UT and lasted ~1 hour. The middle panel of Plate 2 shows assimilated data acquired ~15 min after the onset of this expansion. By this time, Poker Flat had become visible to the Polar satellite. The western boundary of the VIS image, running through the Alaskan settlements of Anchorage and Kotzebue, indicates the limit of the field of view of the imager.

Both the ASC and VIS images show discrete aurora equatorward of Poker Flat, as expected from the equatorward expansion seen in the MSP data. As in the upper panel of Plate 2, the ASI-FPS once again observed geomagnetically westward winds coincident with this discrete aurora. However, having followed the equatorward auroral expansion, the westward neutral flow now also lay south of Poker Flat. The geomagnetically southernmost arrows in the ASI-FPS data indicate that the east-to-west wind shear (with increasing latitude) that was seen at 0601 UT was probably still present in the F region wind field, although it now lay so far south that the strongest of this shear had left the ASI-FPS field of view. In the north, by contrast, the westward neutral flow ended at a sharp shear line just north of Poker Flat. This shear in the north, which had the opposite sense to that in the south, lay spatially coincident with the poleward boundary of the discrete aurora. The reason for the shear in the north is apparent from the inferred plasma convection profile. Near the northern limit of the ASI-FPS field of view, plasma convection had already turned eastward. The neutral wind in that locale had not yet fully reversed (to flow eastward), but the westward flow had waned. This behavior is consistent with the expectation that the neutral wind will mimic the ion convection, at least to some extent, but with a response delayed by 30-60 min.

4.5. 0804 UT

At 0804 UT, 3 hours before magnetic midnight, the images from Polar, Poker Flat, and Kaktovik indicate that a large spiral feature had formed in the aurora over Alaska (lower panel of Plate 2). Compared to 0644 UT, the aurora had also receded poleward. The channel of westward neutral flow followed the aurora's poleward retreat, so that the westward winds occurred directly over Poker Flat.

The east-to-west shear of zonal wind with latitude

that had prevailed above Poker Flat at 0601 UT was once again visible in the south. Near the northern edge of the ASI-FPS field of view, the magnetometers continued to show the eastward convection that was seen at 0644 UT. The diminished westward neutral wind in the geomagnetic north suggests that eastward momentum was being transferred from ions to neutrals at these latitudes.

The assimilated data maps thus indicate that westward wind in the evening sector occurred in a latitudinally confined channel, as has been reported by previous authors [e.g., *Rees et al.*, 1985; *Killeen et al.*, 1988]. The large auroral spiral at 0804 UT may have been associated with the west-to-east plasma convection reversal seen north of Poker Flat by the magnetometers.

4.6. 0919 UT

By 0919 UT, the ASC and VIS images in the upper panel of Plate 3 indicated that the brightest discrete auroral arcs had moved south of Poker Flat. This transition is also apparent in Figure 3, where the MSP record shows that the brightest discrete aurora then remained continuously south of Poker until ~1215 UT. The equatorward auroral expansion placed Poker Flat inside the auroral oval. Successive ASI-FPS exposures from this time clearly illustrate the neutral wind response to this transition.

With the aurora southward of Poker Flat, magnetometers to the north began observing stronger eastward convection inside the auroral oval. The ASI-FPS wind field at 0919 UT shows that the wind north of Poker Flat had also turned eastward, whereas westward flow continued to prevail far to the south. The resulting wind field was highly curved and sheared but in a sense that was almost a mirror reversal (about the magnetic meridian) of the flow pattern depicted in the upper panel of Plate 2 for the conditions at 0601 UT.

4.7. 0932 UT

ASC and VIS images in the middle panel of Plate 3, corresponding to a time of 0932 UT, indicate that the aurora had brightened considerably during the 13 min since the situation depicted in the upper panel, although it remained approximately stationary in geographic location. The eastward ion convection had advanced equatorward, so that eastward convection was now occurring well south of Poker Flat. The wind response lagged behind that of the ion convection. That is, while eastward neutral flow did advance equatorward noticeably, and west-to-east wind shear became sharper, the region of eastward wind did not advance as far as the ion convection had.

4.8. 0946 UT

The lower panel of Plate 3, corresponding to a time of 0946 UT, shows that the aurora remained both bright and in approximately the same location as in the two panels above. While the equatorward edge of the eastward ion convection had not moved much, the centroid latitude of the eastward convection did advance south. The ASI-FPS data show that while the wind shear front continued to advance southward, it also continued to "lag" behind the southward advance of eastward ion convection. The clockwise wind field curvature that was apparent in the previous two exposures had begun to weaken significantly by this time, at least for the portion of the wind field within our field of view.

4.9. 1019 UT

By 1019 UT the ASC and VIS images, shown in the upper panel of Plate 4, indicate that the main auroral oval still remained south of Poker Flat, as in Plate 3. While there was a bright region in western Canada near Great Slave Lake, the aurora had faded somewhat over most of the spacecraft image, compared to 0946 UT. (Although not shown here, we generated an assimilation map corresponding to 0959 UT, and it also shows generally fainter aurora prevailed compared to 0946 UT.) The magnetometer chain indicated that eastward ion convection now prevailed at virtually all latitudes across interior Alaska, although with a slightly decreased amplitude relative to the previous few cases. The shear front in the neutral wind field had continued its advance equatorward. Now, clockwise curvature was almost entirely absent from the ASI-FPS field of view, and eastward neutral flow covered all but its southernmost edge.

4.10. 1046 UT

The middle panel of Plate 4, corresponding to a time of 1046 UT, shows the final outcome of the transition that commenced at just after 0900 UT. The ASC and VIS images show that the aurora brightened again and expanded poleward by a few hundred kilometers. The thermospheric wind was now blowing geomagnetically eastward throughout the ASI-FPS field of view. Nevertheless, some shear with latitude remained; the flow speed of ~180 $\mathrm{m\,s^{-1}}$ near the northernmost viewing zones was approximately double that in the southernmost zones.

4.11 1303 UT

All of the previous panels in Plates 2-4 have corresponded to times prior to magnetic midnight, which occurs at ~1120 UT at Poker Flat. The lower panel of Plate 4, corresponding to a time of 1303 UT, shows the aurora, inferred convection, and ASI-FPS wind field ~100 min after magnetic midnight. The Kaktovik ASC had shut down by this time. The Poker Flat ASC and Polar-VIS images show that the aurora had receded poleward and once again lay north of Poker Flat. (The MSP data in Figure 3 indicate the aurora actually receded poleward ~45 min earlier, at ~1215 UT.) The ion convection profile shows a "bite-out" in latitudes south

of Poker Flat. This is probably indicative of a general poleward movement of the zone of eastward ion drift, as expected in the postmidnight sector.

Despite bright aurora and a continued strong electrojet, the wind field at 1303 UT was relatively uniform. A slight curvature was evident and perhaps some acceleration of the flow as it passed across our field of view. However, there were no obvious small-scale flow features that appeared to be associated either with the visible aurora or with the ion convection. Further, the flow direction was now rotated by ~45° with respect to the auroral oval. This contrasts with the geometries observed before midnight, when bright aurora in our field of view tended to be associated with winds blowing roughly parallel to the oval. This rotation away from the magnetic east-west alignment had occurred as a smooth transition during the time since magnetic midnight. Our database of ASI-FPS wind measurements shows that the postmidnight wind field over Poker Flat is often dominated by uniform antisunward flow, as the cross-polar jet emerges from the polar cap on the nightside. The cross-polar jet is driven by the solar pressure gradient and ion-drag forces acting together to accelerate polar cap air parcels antisunward. Apparently, this large-scale wind feature usually overwhelms any local coupling effects occurring near Poker Flat after midnight.

5. Discussion

Although our assimilation maps are purely qualitative, we believe they are nevertheless an extremely powerful tool for exposing the physical processes coupling the Earth's magnetosphere, ionosphere, and neutral thermosphere. Their usefulness is due not just to the assimilation of multiple data sources. Of equal importance in this case is that three of the four contributing experiments resolved their measurements over two horizontal spatial dimensions, while the fourth resolved over one spatial dimension. Thus, for example, we are able here to distinguish between spatial and temporal variations in the wind field, which would have been impossible with just a time series of single-point wind vector measurements.

In assembling the maps presented here (plus others for this same night), we were immediately struck by the consistency between the various data sets. Wind shears were clearly associated with the aurora and its latitudinal boundaries. When the aurora moved in latitude, so to did the corresponding shear zones. Further, both the wind shears and the auroral brightness distribution correlated well with the ion-drift profile that we inferred from the electrojet calculation. This latter association is strongly supportive of ion drag as the mechanism that establishes the coupling.

This study was in many ways similar to that performed by *Killeen et al.* [1988]. Those authors used data from the Dynamics Explorer 1 and 2 satellites to assimilate neutral wind vectors, zonal ion drift speeds, hemispheric-scale auroral images, ion densities, and neutral composition. Many of their major findings are also supported or complemented by our own results. In particular, we fully concur with *Killeen et al.*'s [1988, p. 2680] conclusion that "a strong gradient in sunward flow speed is located at the equatorward edge of the auroral oval in the dusk sector and that a weaker gradient, of opposite sign, is associated with the poleward edge of the oval." They also noted [p. 2688] that "there are significant differences between the locations of boundaries in the neutral and ion flows," and they postulated that these offsets could arise because of the relatively long time constants for ion-neutral momentum transfer. That is, the rapid changes in the ion convection pattern would lead any corresponding neutral response. Unfortunately, the DE 2 satellite orbit prevented it from observing any single location for an extended period of time. Thus, *Killeen et al.* [1988] could not observe the time evolution of neutral and ion flows to test this hypothesis.

In our case, however, the ground-based instruments did observe the same region throughout the entire night. Similarly, the Polar spacecraft orbit allowed for many hours of continuous images over Alaska. Observations from 0919 to 1019 UT show that changes in the neutral wind occurred as a time-lagged response to changes in ion convection which, in turn, lagged behind changes in the location of auroral precipitation. During the period when the neutral wind appeared to be responding to changed forcing, we did observe displacements between neutral and ion flow boundaries, exactly as was suggested by *Killeen et al.* [1988].

Our observations clearly show a feature of the duskside neutral wind field that corresponds to "the westward thermospheric jet-stream of the evening auroral oval" described, for example, by *Rees et al.* [1985]. However, we did not observe the "typical" speeds of 200-500 $\mathrm{m\,s^{-1}}$ suggested by those authors, let alone the speeds in excess of 800 $\mathrm{m\,s^{-1}}$ that they observed in extreme cases. Rather, the speeds we observed were more typically 100-150 $\mathrm{m\,s^{-1}}$. We consider this to be a consequence of the solar minimum conditions, the winter season, and the auroral and magnetic conditions prevailing during the hours preceding dusk at our location. Stronger westward neutral flow can be observed in the evening at Poker Flat during solar minimum; however, this usually takes several hours of storm level activity prior to dusk, to "spin-up" the thermosphere's high-latitude duskside circulation cell. Subsequent Poker Flat ASI-FPS observations during 1998 and 1999 have shown that dusk sector F region wind speeds of 400-500 $\mathrm{m\,s^{-1}}$ have indeed become more common, as the $F_{10.7}$ index has increased with rising solar activity.

Finally, we believe that our comparison between data sets was also useful for validating the vector wind fields inferred from the ASI-FPS. Both the ASI-FPS instrument itself and the analysis procedure used to derive

vector wind fields are relatively new. We do not have a second independent technique for F region vector wind mapping that we could use for direct validation of the ASI-FPS results. However, the consistency between these wind fields and other spatially resolved geophysical data greatly increases our confidence in the ASI-FPS observations and analysis methods.

6. Conclusions

We have examined the spatial relationships between the aurora, ionospheric plasma convection, and the F region wind field, for the night of February 10, 1997. The major conclusions are as follows. Before midnight, geomagnetically westward directed ion convection drove a latitudinally confined channel of geomagnetically westward wind, in opposition to the pressure gradient established by solar heating. The westward wind channel was bounded by strong latitudinal shear on both its equatorward and poleward sides. The westward flow channel and shear zones were spatially associated with auroral boundaries seen in images from both the Polar spacecraft and the ground-based all-sky camera. The shear zones also correlated well with shear in the electrojet-inferred F region plasma convection. The westward wind itself maximized either within the discrete aurora or near its equatorward edge. Shear on the equatorward side of the flow maximized within the diffuse aurora.

On the poleward side, and in the early evening hours, shear maximized near the poleward edge of the discrete aurora. The shear poleward of the discrete aurora marked the transition to antisunward neutral flow within the polar cap. When the aurora expanded equatorward just after 0900 UT, the polar cap neutral flow followed, as was indicated by the equatorward advance of the region of eastward wind between 0919 and 1019 UT. The neutral wind response lagged behind that of the ion convection, in the sense that for a given time during this transition, eastward ion convection was seen several hundred kilometers farther equatorward than eastward neutral flow.

However, as local time progresses from dusk toward magnetic midnight, the polar cap flow typically encounters the auroral oval at ever steeper angles, and so the polar cap flow becomes progressively more likely to "spill" across the oval and subsequently penetrate to lower latitudes. Thus the equatorward advance of the eastward wind did not stop when it "caught-up" with the equatorward expansion of the auroral oval (at around 1019 UT). By 1046 UT polar cap neutral flow covered Alaska, and by 1303 UT the postmidnight wind field was dominated by the emergence of the cross-polar jet from the polar cap. This appeared to overwhelm any wind features associated with local auroral processes.

Acknowledgments. This work was supported by NSF grant ATM-9523810. One of us (J.D.C.) was supported by NASA grant NAG 5-8042 and by a subcontract (University of Iowa V95254) to the University of Iowa's NASA contract NAS 5-30316. We thank June Pelehowski for supporting the operation of the Fabry-Perot spectrometer, all-sky camera, magnetometers, and the observatory at Poker Flat. The IMF data shown in Figure 4 were recorded by the MFI instrument aboard the Wind spacecraft, and they were provided courtesy of R. Lepping and NASA Goddard Spaceflight Center. Access to these data was facilitated by NASA's "CDAWeb" World Wide Web site (http://cdaweb.gsfc.nasa.gov/). Janet G. Luhmann thanks John W. Meriwether and Delores Knipp for their assistance in evaluating this paper.

References

Bates, H. F., and T. D. Roberts, The southward midnight surge in F -layer wind observed with the Chatanika incoherent scatter radar, *J. Atmos. Terr. Phys.*, *39*, 87-93, 1977.

Biondi, M.A., D.P. Sipler, M.E. Zipf, and J.L. Baumgardner, All-sky Doppler interferometer for thermospheric dynamics studies, *Appl. Opt.*, *39*, 1646-1654, 1995.

Burnside, R. G., F. A. Herrero, J. W. Meriwether Jr., and J. C. G. Walker, Optical observations of thermospheric dynamics at Arecibo, *J. Geophys. Res.*, *86*, 5532-5540, 1981.

Chang, C. A., and J.-P. St.-Maurice, Two-dimensional high-latitude thermospheric modeling: A comparison between moderate and extremely disturbed conditions, *Can. J. Phys.*, *69*, 1007-1031, 1991.

Conde, M., and R. W. Smith, Mapping thermospheric winds in the auroral zone, *Geophys. Res. Lett.*, *22*, 3019-3022, 1995.

Conde, M., and R. W. Smith, Phase compensation of a separation scanned, all-sky imaging Fabry-Perot spectrometer for auroral studies, *Appl. Opt.*, *36*, 5441-5450, 1997.

Conde, M., and R. W. Smith, Simultaneous observations of the aurora and of non-uniform thermospheric winds, from Poker Flat, Alaska, Proc. NIPR Symp. Upper Atmos. Phys., *12*, 30-38, 1998a.

Conde, M., and R. W. Smith, Spatial structure in the thermospheric horizontal wind above Poker Flat, Alaska, during solar minimum, *J. Geophys. Res.*, *103*, 9449-9472, 1998b.

Dickinson, R., E. C. Ridley, and R. G. Roble, A three dimensional general circulation model of the thermosphere, *J. Geophys. Res.*, *86*, 1499-1512, 1981.

Frank, L. A., J. B. Sigwarth, J. D. Craven, J. P. Cravens, J. S. Dolan, M. R. Dvorsky, P. K. Hardebeck, J. D. Harvey, and D. W. Muller, The Visible Imaging System (VIS) for the Polar spacecraft, *Space. Sci. Rev.*, *71*, 297-328, 1995.

Fuller-Rowell, T. J., A two-dimensional, high-resolution, nested-grid model of the thermosphere, 2, Response of the thermosphere to narrow and broad electrodynamic features, *J. Geophys. Res.*, *90*, 6567-6586, 1985.

Fuller-Rowell, T. J., and D. Rees, A three dimensional time dependent model of the thermosphere, *J. Atmos. Sci.*, *37*, 2545- 2567, 1980.

Fuller-Rowell, T. J., D. Rees, S. Quegan, R. J. Moffett, and G. J. Bailey, Interactions between neutral thermospheric composition and the polar ionosphere using a coupled ionosphere-thermosphere model, *J. Geophys. Res.*, *92*, 7744-7748, 1987.

Hays, P. B., J. W. Meriwether Jr., and R. G. Roble, Nighttime thermospheric winds at high latitudes, *J. Geophys. Res.*, *84*, 1905-1913, 1979.

Hays, P. B., T. L. Killeen, N. W. Spencer, L. E. Wharton, R. G. Roble, B. A. Emery, T. J. Fuller-Rowell, D. Rees, L. A. Frank, and J. D. Craven, Observations of the dynamics of the polar thermosphere, *J. Geophys. Res.*, *89*, 5597-5612, 1984.

Heppner, J. P., and M. L. Miller, Thermospheric winds at

high latitudes from chemical release observations, *J. Geophys. Res.*, *87*, 1633-1647, 1982.

Idenden, D. W., R. J. Moffett, S. Quegan, and T. J. Fuller-Rowell, Time-dependent convection at high latitudes, *Ann. Geophys.*, *14*, 1159-1169, 1996.

Keskinen, M. J., and P. Satyanarayana, Nonlinear unstable auroral-arc driven thermospheric winds in an ionosphere-magnetosphere coupled model, *Geophys. Res. Lett.*, *20*, 2687-2690, 1993.

Killeen, T. L., and R. G. Roble, Thermosphere dynamics: Contributions from the first 5 years of the Dynamics Explorer program, *Rev. Geophys.*, *26*, 329-367, 1988.

Killeen, T. L., P. B. Hays, G. R. Carignan, R. A. Heelis, W. B. Hanson, N. W. Spencer, and L. H. Brace, Ion-neutral coupling in the high latitude *F* region: Evaluation of the ion heating terms from Dynamics Explorer 2, *J. Geophys. Res.*, *89*, 7495-7508, 1984.

Killeen, T. L., J. D. Craven, L. A. Frank, J. J. Ponthieu, N. W. Spencer, R. A. Heelis, L. H. Brace, R. G. Roble, P. B. Hays, and G. R. Carignan, On the relationship between dynamics of the polar thermosphere and morphology of the aurora: Global-scale observations from Dynamics Explorers 1 and 2, *J. Geophys. Res.*, *93*, 2675-2692, 1988.

Kimball, J., and T. J. Hallinan, A morphological study of black vortex streets, *J. Geophys. Res.*, *103*, 14,683-14,695, 1998a.

Kimball, J., and T. J. Hallinan, Observations of black auroral patches and of their relationship to other types of aurora, *J. Geophys. Res.*, *103*, 14,671-14,682, 1998b.

Larsen, M. F., T. R. Marshall, I. S. Mikkelsen, B. A. Emery, A. Christensen, D. Kayser, J. Hecht, L. Lyons, and R. Walterscheid, Atmospheric response in aurora experiment: Observations of *E* and *F* region neutral winds in a region of postmidnight diffuse aurora, *J. Geophys. Res.*, *100*, 17,299-17,308, 1995.

Larsen, M. F., A. B. Christensen, and C. D. Odom, Development of unstable atmospheric layers near 100 km in the postmidnight auroral oval, *Geophys. Res. Lett.*, *24*, 1915-1918, 1997.

Lyons, L. R., and R. L. Walterscheid, Generation of auroral omega bands by shear instability of the neutral winds, *J. Geophys. Res.*, *90*, 12,321-12,329, 1985.

Meriwether, J. W., Jr., J. P. Heppner, J. D. Stolarik, and E. M. Wescott, Neutral winds above 200 km at high latitudes, *J. Geophys. Res.*, *78*, 6643-6661, 1973.

Meriwether, J. W., Jr., T. L. Killeen, F. G. McCormac, A. G. Burns, and R. G. Roble, Thermospheric winds in the geomagnetic polar cap for solar minimum conditions, *J. Geophys. Res.*, *93*, 7478-7492, 1988.

Mikkelsen, I. S., T. S. Jorgensen, M. C. Kelley, M. F. Larsen, E. Pereira, and J. Vickrey, Neutral winds and electric fields in the dusk auroral oval, 1, Measurements, *J. Geophys. Res.*, *86*, 1513-1524, 1981.

Nagy, A. F., R. J. Cicerone, P. B. Hays, K. D. McWatters, J. W. Meriwether Jr., A. E. Belon, and C. L. Rino, Simultaneous measurements of ion and neutral motions by radar and optical techniques, *Radio Sci.*, *9*, 315-321, 1974.

Nakajima, H., S. Okano, H. Fukunishi, and T. Ono, Observations of thermospheric wind velocities and temperatures by the use of a Fabry-Perot Doppler imaging system at Syowa Station, Antarctica, *Appl. Opt.*, *34*, 8382-8395, 1995.

Rees, D., and A. H. Greenaway, Doppler imaging system: An optical device for measuring vector winds, 1, General principles, *Appl. Opt.*, *22*, 1078-1083, 1983.

Rees, D., T. J. Fuller-Rowell, M. F. Smith, R. Gordon, T. L. Killeen, P. B. Hays, N. W. Spencer, L. Wharton, and N. C. Maynard, The westward thermospheric jet stream of the evening auroral oval, *Planet. Space Sci.*, *33*, 425-456, 1985.

Richmond, A. D., E. C. Ridley, and R. G. Roble, A thermosphere ionosphere general circulation model with coupled electrodynamics, *Geophys. Res. Lett.*, *19*, 601-604, 1992.

Roble, R. G., and E. C. Ridley, An Auroral model for the NCAR thermospheric general circulation model, *Ann. Geophys.*, *5*, 369-382, 1987.

Roble, R. G., E. C. Ridley, A. D. Richmond, and R. E. Dickinson, A coupled thermosphere ionosphere general circulation model, *Geophys. Res. Lett.*, *15*, 1325-1328, 1988.

Sica, R. J., M. H. Rees, G. J. Romick, G. Hernandez, and R. G. Roble, Auroral zone thermospheric dynamics, 1, Averages, *J. Geophys. Res.*, *91*, 3231-3244, 1986a.

Sica, R. J., M. H. Rees, R. G. Roble, G. Hernandez, and G. J. Romick, The Altitude region sampled by ground based Doppler temperature measurements of the OI 15867 K emission line in aurorae, *Planet. Space Sci.*, *34*, 483-488, 1986b.

Sica, R. J., G. Hernandez, B. A. Emery, R. G. Roble, R. W. Smith, and M. H. Rees, The control of auroral zone dynamics and thermodynamics by the interplanetary magnetic field dawn-dusk (Y) component, *J. Geophys. Res.*, *94*, 11,921-11,932, 1989.

Sica, R. J., J.-P. St.-Maurice, G. Hernandez, G. J. Romick, and R. Tsunoda, Computations of local ion energy balance in the auroral zone, *J. Geophys. Res.*, *98*, 15,667-15,676, 1993.

Smith, R. W., D. Rees, and R. D. Stewart, Southern hemisphere thermospheric dynamics: A review, *Rev. Geophys.*, *26*, 591-622, 1988.

Smith, R. W., J. W. Meriwether Jr., G. Hernandez, D. Rees, V. Wickwar, O. de la Beaujardiere, and T. L. Killeen, Mapping the wind in the polar thermosphere: A case study within the CEDAR program, *Eos Trans. AGU*, *70*, 161, 1989.

Spencer, N. W., L. E. Wharton, G. R. Carignan, and J. C. Maurer, Thermosphere zonal winds, vertical motions and temperature as measured from Dynamics Explorer, *Geophys. Res. Lett.*, *9*, 953-956, 1982.

St.-Maurice, J. P., and R. W. Schunk, Ion-neutral momentum coupling near discrete high-latitude ionospheric features, *J. Geophys. Res.*, *86*, 11,299-11,321, 1981.

Sun, W., Y. Kamide, J. R. Kan, and S.-I. Akasofu, Inversion of the auroral electrojets from magnetometer chain data based on the flexible tolerance method, *J. Geomagn. Geoelectr.*, *45*, 1151-1157, 1993.

Walterscheid, R. L., and L. R. Lyons, The neutral circulation in the vicinity of a stable auroral arc, *J. Geophys. Res.* ,*97*, 19,489-19,499, 1992.

Walterscheid, R. L., L. R. Lyons, and K. E. Taylor, The perturbed neutral circulation in the vicinity of a symmetric stable auroral arc, *J. Geophys. Res.*, *90*, 12,235-12,248, 1985.

Weimer, D. R., Models of high-latitude electric potentials derived with a least error fit of spherical harmonic coefficients, *J. Geophys. Res.*, *100*, 19,595-19,607, 1995.

Wickwar, V. B., J. W. Meriwether, P. B. Hays, and A. F. Nagy, The meridional thermospheric neutral wind measured by radar and optical techniques in the auroral region, *J. Geophys. Res.*, *89*, 10,987-10,998, 1984.

M. Conde, J. D. Craven, T. Immel, E. Hoch, H. Stenbaek-Nielsen, T. Hallinan, R. W. Smith, J. Olson and Wei Sun, Geophysical Institute, University of Alaska, 903 Koyukuk Drive, P.O. Box 757320, Fairbanks, Alaska, 99775-7320. (mark.conde@gi.alaska.edu)

L. A. Frank and J. Sigwarth, Department of Physics and Astronomy, University of Iowa, Iowa City, IA, 52242.

(Received April 12, 2000; revised July 12, 2000; accepted July 12, 2000.)